Origin of traps and charge transport mechanism in hafnia

D. R. Islamov, V. A. Gritsenko, C. H. Cheng, and A. Chin

Origin of traps and charge transport mechanism in hafnia

D. R. Islamov,[1,2,a)] V. A. Gritsenko,[1,2,b)] C. H. Cheng,[3] and A. Chin[4,c)]

[1]*Rzhanov Institute of Semiconductor Physics, Siberian Branch of Russian Academy of Sciences, Novosibirsk 630090, Russian Federation*
[2]*Novosibirsk State University, Novosibirsk 630090, Russian Federation*
[3]*Department of Mechatronic Technology, National Taiwan Normal University, Taipei 106, Taiwan*
[4]*National Chiao Tung University, Hsinchu 300, Taiwan*

In this study, we demonstrated experimentally and theoretically that oxygen vacancies are responsible for the charge transport in HfO_2. Basing on the model of phonon-assisted tunneling between traps, and assuming that the electron traps are oxygen vacancies, good quantitative agreement between the experimental and theoretical data of current-voltage characteristics was achieved. The thermal trap energy of 1.25 eV in HfO_2 was determined based on the charge transport experiments. © 2014 AIP Publishing LLC. [http://dx.doi.org/10.1063/1.4903169]

Knowledge about charge transport mechanisms hafnia (hafnium oxide, HfO_2) is crucial for modern microelectronics, because high-κ HfO_2 is used as a gate dielectric in high-speed MOSFETs[1,2] and FinFETs[3,4] and a blocking insulator in Si-oxide-nitride-oxide-silicon-type (SONOS) flash memory cells.[5,6] Hafnia is a promising candidate to used as active medium in resistive random access memory (RRAM), which would involve combining the most favorable properties of both high-speed dynamic random access memory and non-volatile flash memory.[7–9] Hereby, MOSFETs and SONOS need high-κ dielectrics with low leakage currents, while RRAM requires dielectric medium with reversible resistive switching. Managing the process of hafnia films synthesis to control leakage currents can create high-quality devices for various purposes. However, an unresolved physics is the nature of defects and traps that are responsible for the charge transport in HfO_2. The atomic structure of defect that affects the localization and charge transport still remains unclear. Currently, the accepted hypothesis is that oxygen vacancies are responsible for charge transport in dielectric.[9–11] Although many studies have investigated the theory of the atomic and electronic structure of oxygen vacancies in hafnia,[11–18] direct experimental data regarding the presence of oxygen vacancies in hafnia were reported recently.[19] It was shown that oxygen vacancies in hafnia are responsible for blue luminescence band at 2.7 eV and a luminescence excitation band at 5.2 eV, and a hypothesis that the oxygen vacancies in hafnia act as traps in charge transport through the dielectric was discussed.[19] In this case, thermal energy traps in HfO_2 are equal to a half of the Stokes luminescence shift $W_t = (5.2 - 2.7)/2 = 1.25$ eV.

A lot of studies of the charge transport in dielectrics described experiment results by Poole-Frenkel (PF) mechanism in hafnia-based structures.[20–23] The most part of HfO_2 transport investigations did not get into account neither charge trap density, which depends on thin film fabrication technology, nor phonon influence on electron and hole transport, which might be significant at high temperatures. Only few of investigations explained their results quantitatively as well as qualitatively, getting agreement of the phenomenological parameters such as dynamic permittivity, trap energy, frequency factor, etc. However, these studies involved complex mathematical calculations.[24]

In this letter, phonon-assisted tunneling between traps (PATT) conduction mechanism in HfO_2 was developed. Proposed model has simple mathematics and is in good quantitative and qualitative agreement with experimental data. It was clearly shown that oxygen vacancies are responsible for the charge transport in HfO_2 and HfO_2-based devices.

Transport measurements were performed for metal-insulator-semiconductor (MIS) and metal-insulator-metal (MIM) structures. For the MIS $Si/HfO_x/Ni$ structures, the 20-nm-thick amorphous hafnia was deposited on a n-type Si (1 0 0) wafer by using the atomic layer deposition (ALD) system. Tetrakis dimethyl amino hafnium (TDMAHf) and water vapor were used as precursors at a chamber temperature of 250 °C for HfO_x film deposition.

Another set of MIS samples with 8-nm-thick HfO_x films was fabricated using physical vapor deposition (PVD). A pure HfO_2 target was spattered by an electron beam, and HfO_2 was deposited on the n-type Si (1 0 0) wafer. Low temperature post-deposition annealing (PDA) during 15 min at 400 °C was applied to prevent the growth of interfacial SiO_x.[25] Structural analysis shows that the resulting HfO_x films were amorphous. To fabricate $Si/TaN/HfO_x/Ni$ MIM structures, we deposited the 8-nm-thick amorphous hafnia on 100-nm-thick TaN films on Si wafers, using PVD. We did not apply any post-deposition annealing to produce the most non-stoichiometric films. All samples for transport measurements were equipped with round 50-nm-thick Ni gates with a radius of 70 μm. Transport measurements were performed using a Hewlett Packard 4155B semiconductor parameter analyzer and an Agilent E4980A precision LCR meter.

The experimental current-voltage (I-V) characteristics in MIS(PVD) structures, measured at different temperatures T with a positive bias applied to the Ni contact, are shown in Fig. 1, graphed by different characters in PF $(\log(I) - \sqrt{V})$ plot. The current grows exponentially with increasing of the

a)Electronic mail: damir@isp.nsc.ru
b)Electronic mail: grits@isp.nsc.ru
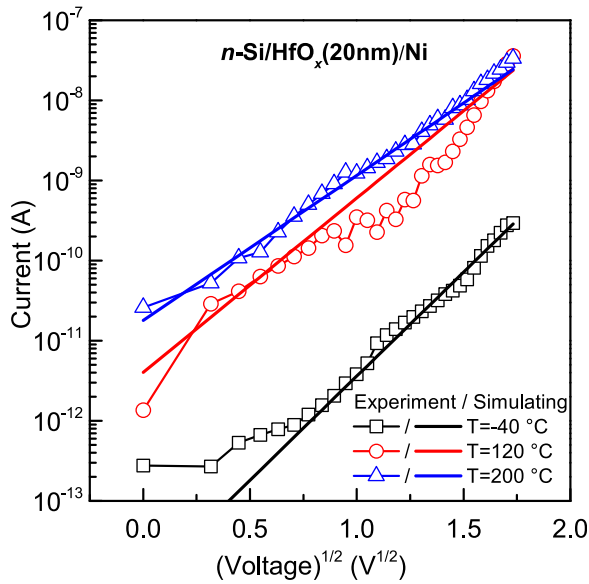c)Electronic mail: albert_achin@hotmail.com

FIG. 1. Experimental current-voltage characteristics (characters) of *n*-Si/HfO$_x$/Ni MIS(PVD) structure and simulation (lines) by Frenkel model of the trap ionization (1) and (2) at different temperatures on PF plot.

gate voltage and temperature. We attempted to explain the experimental data by using isolated trap ionization model

$$J = eN^{2/3}P, \qquad (1)$$

where J is the current density, e is the electron charge, N is the charge trap density, P is the probability of trap ionization per second and has different dependencies on electric field F and temperature. In term of PF model, the probability is

$$P = \nu \exp\left(-\frac{W_t - \beta_{PF}\sqrt{F}}{kT}\right), \qquad (2)$$

ν is the frequency factor which was defined as $\nu \simeq W_t/h$, W_t is thermal trap energy (the energy of thermal ionization of the trap), h is the Planck constant, β_{PF} is Poole-Frenkel coefficient, F is the electric field, and k is the Boltzmann constant.[26] Experimental *I-V* characteristics and results of the fitting procedure are shown in Fig. 1. As can be seen, Frenkel model (2) describes the experiment data qualitatively very good. However, quantitative fitting procedure returns nonphysical fitting parameter values: the slopes of the fitting lines with Poole-Frenkel coefficient $\beta_{PF} = \sqrt{e^3/\pi\varepsilon_0\varepsilon_\infty}$ give the dynamic permittivity $\varepsilon_\infty(T) = 10$–$20$, which is much higher than $\varepsilon_\infty(HfO_2) = 4$. ε_0 is vacuum permittivity (dielectric constant). Further fittings return $N \sim 4$ cm^{-3} and $W_t = 0.3$–0.4 eV. Found value, the charge trap density of $N \sim 4$ cm^{-3} at $\nu \simeq W_t/h \sim 10^{14}$ s^{-1}, corresponds to one trap per ~ 2600 Ni contacts, thus this is unrealistic value. Taking these into account, it was concluded that despite the fact that PF model describes the experiment data qualitatively, there is no quantitative agreement between experiments and theory. We tried to describe our experiments with other charge transport models in dielectrics, Hill model of overlapped traps ionization,[27] and the model of multiphonon trap ionization.[28] However, the fitting procedures involved in these models returned the nonphysical fitting parameter values as well as PF model.

To describe the experiments quantitatively and qualitatively, we performed simulations based on the PATT model.[29] In this model, the probability of electron tunneling between traps per second is defined as following:

$$P = \frac{\sqrt{2\pi}\hbar W_t}{m^* s^2 \sqrt{W_{opt} - W_t}} \exp\left(-\frac{W_{opt} - W_t}{2kT}\right)$$
$$\times \exp\left(-\frac{2s\sqrt{m^* W_t}}{\hbar}\right)\sinh\left(\frac{eFs}{2kT}\right),$$
$$kT \ll W_t, \quad eFs \ll W_t, \qquad (3)$$

$\hbar = h/2\pi$, W_{opt} is the energy of optical excitation of the trap, m^* is the effective mass, and $s = N^{-1/3}$ is mean distance between traps. The results of this multi-parameter fitting procedure are shown in Fig. 2, graphed in solid lines. This procedure yielded the values of different transport parameters, $N = 6.8 \times 10^{19}$ cm^{-3}, $W_t = 1.25$ eV, $W_{opt} = 2W_t = 2.5$ eV, and $m^* = (0.3$–$0.4)m_e$ (m_e is a free electron mass). Quantitatively, there is full agreement between the PATT model and the experimental data. The trap thermal energy value of 1.25 eV that was obtained is close to that of 1.2 eV (Ref. 30) and $W_t = 1.36$ eV (Ref. 24) observed earlier, and equal to a half of the Stokes luminescence shift.[19]

Furthermore, the trap optical energy value of $W_{opt} = 2.5$ eV is close to the calculated value of 2.35 eV for the negatively charged oxygen vacancy in hafnia reported earlier.[15]

Fig. 3 shows the configuration diagram of a negatively charged oxygen vacancy (electron trap) in hafnia. A vertical transition with a value of 2.5 eV corresponds to the optical trap excitation, and transitions of 1.25 eV correspond to thermal trap energy.

The inset in Fig. 2 show experimental capacitance-voltage characteristics of the MIS(PVD) structure at different voltage limits. Positions of the right hysteresis branch of *C-V* characteristics depend on the voltage limits, while the left

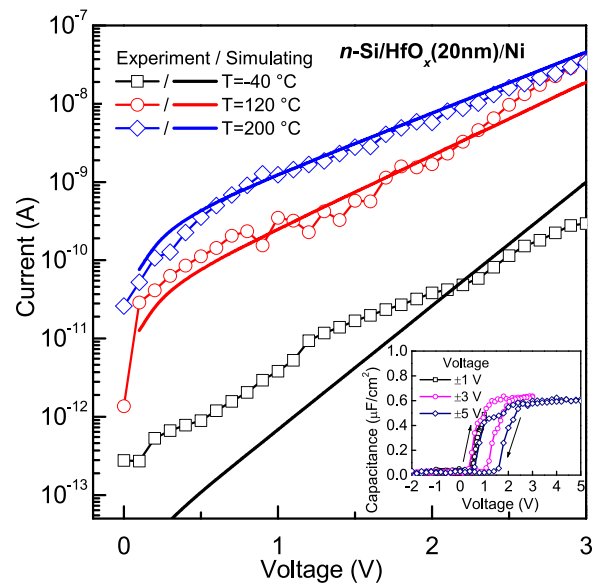FIG. 2. Experimental current-voltage characteristics (characters) of *n*-Si/HfO$_x$/Ni MIS(PVD) structure and simulation (lines) by PATT model (3) at different temperatures. Inset: experimental capacitance-voltage characteristics of the MIS(PVD) structure at different voltage limits; arrows show sweep voltage directions.
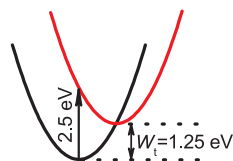
FIG. 3. Configuration coordination energy diagram of trap ionization process on negative charged oxygen vacancy in hafnia (lower term is filled ground state, upper term is excited empty state).

branch is fixed. Sweep voltage directions show that the bulk charge is accumulating on the traps with the voltage growing. These phenomena show that the electron traps are filled only, while the holes traps (if any) are empty. Voltage loop allows us to valuate the density of the filled electron traps n_e $\lesssim 3.7 \times 10^{18}$ cm^{-3}, which is less than 20 times than found value of N.

The same procedure was applied to experiment data of the charge transport measurements in MIS(ALD) and MIM structures. Experiment current-voltage characteristics compared with simulations in terms of the PATT model in MIS(ALD) are shown in Fig. 4. Fitting procedure returns the following parameters values: $N = 2.5 \times 10^{20}$ cm^{-3}, $W_t = 1.25$ eV, $W_{opt} = 2W_t = 2.5$ eV, and $m^* = 0.8 \, m_e$. Different values of fitting parameters of MIS(ALD) and MIS(ALD) structures have only the trap density N and effective mass m^*. The difference of effective mass values is due to bulk space charge (due to captured in traps electrons and holes), which is adequately addressed in Ref. 31. Neither thermal trap energy nor optical trap energy depends on film fabrication technology.

The inset in Fig. 4 shows experimental capacitance-voltage characteristics of the MIS(ALD) structure at different voltage limits. With increasing of the voltage limits, the right hysteresis branch of C-V characteristics moves right,
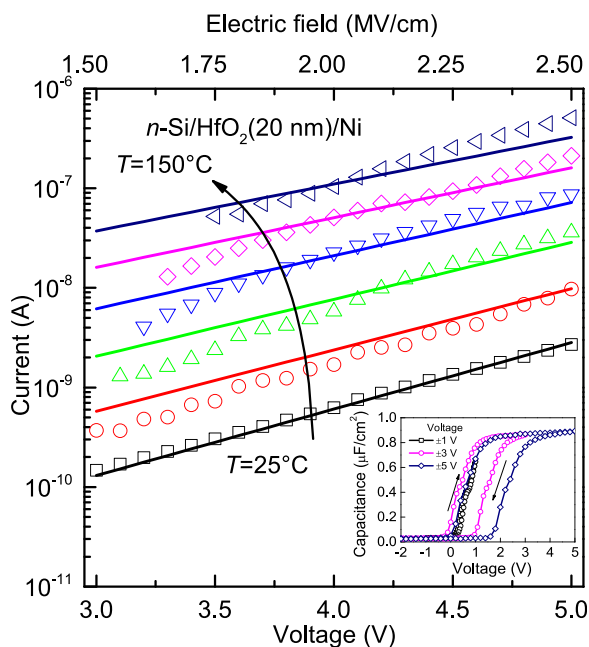
and the left branch moves left. Using the voltage shifts, one can valuate the density of the filled holes and electron traps: $5n_h \approx n_e \lesssim 1.1 \times 10^{19}$ cm^{-3}, respectively. It should be noted that $n_e \approx N/20$ as well as for MIS(PVD) structures.

The bulk charge due to trapped charge carriers blocks the carriers injections from the semiconductor and metal electrodes at low voltages and leads to deviation of simulated $I(V, T)$ from experiment data. To simplify Fig. 4, the mismatched data at $V < 3$ V are not shown. To get full agreement of simulations with experimental data, the bulk charge must be taken into account in solving of Poisson's equation with Shockley-Read-Hall equations for electrons and holes.[31]

Fig. 5 shows the experimental data of current-voltage measurements in MIM structures at different temperatures. The solid lines present the results of simulations in terms of PATT model (3). MIM structures have the following parameter values: $N = 5.5 \times 10^{20}$ cm^{-3}, $W_t = 1.25$ eV, $W_{opt} = 2W_t = 2.5$ eV, and $m^* = 0.9 \, m_e$.

An artifact feature of experimental I-V-T curves shows that the zero current is observed at nonzero but negative voltages as shown in Fig. 5. This phenomenon is due to displacement current

$$I_D = C \cdot dV/dt, \qquad (4)$$

C is capacity of the sample and $dV/dt = +0.3$ V/s is voltage sweep rate. Taking into account (4) in simulation of I-V-T characteristics (1) and (3) with found fitting parameters, the artifact feature is described with good agreement as shown by dashed lines in Fig. 5.

The difference between different MIS ad MIM structures in effective mass is due to bulk space charge. However, it is important to notice that the trap's energy parameters are invariants of grown structures and film fabrication techniques. Consequently, we found that the nature of charge carrier transport in hafnia and hafnia-based structures is
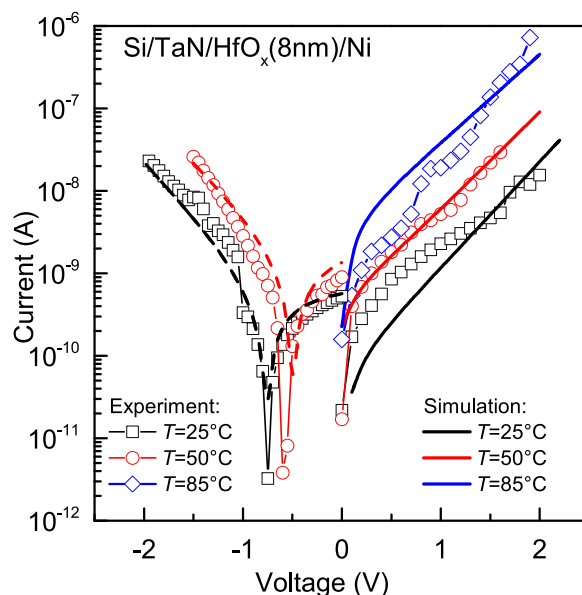

FIG. 4. Experimental current-voltage characteristics (characters) of *n*-Si/HfO$_x$/Ni MIS(ALD) structure and simulation (lines) by PATT model (3) at different temperatures. Inset: experimental capacitance-voltage characteristics of the MIS(ALD) structure at different voltage limits; arrows show sweep voltage directions.

FIG. 5. Experimental current-voltage characteristics (characters) in Si/TaN/HfO$_x$/Ni MIM structures at different temperatures. Black, red, and blue solid lines represent I-V simulations by PATT model at positive bias. Dashed lines show I-V simulations taking into account displacement current (4).

PATT. This charge transport model is more simple than based in quasi-continuous spectra of charge trap energy 1.4–2.4 eV, proposed by Vandelli *et al.*[32]

These results combined with spectra measurements and quantum chemical simulations[19] show that, namely, oxygen vacancies are responsible for charge transport in HfO_x, and the oxygen vacancies play the role of charge traps.

Previous experiments in charge transfer have demonstrated that hafnia conductivity is bipolar (or two-band):[32–34] electrons are injected from a negatively shifted contact in the dielectric, and holes are injected from a positively shifted electrode in the dielectric. For the reason of simplicity, the current study took into account electron conductivity only. This assumption is supported by evaluated values of the filled traps densities, when the holes traps are mostly empty. This means that the hole current is much lower than the electron current caused by blocking holes injection from the metal gate due to high barrier for holes on Ni/HfO_2 interface.[33,35]

To summarize, we examined the transport mechanisms of HfO_2, demonstrating that transport in hafnium oxide is described by the PATT model. Simulating the current-voltage characteristics of this model and comparing experimental data with calculations revealed the energy parameters of the traps in hafnia: the thermal trap energy of 1.25 eV and the optical trap energy of 2.5 eV. PATT charge transport model describes experiment data results with excellent qualitative and quantitative agreement, while standard PF model has qualitative agreement only with unrealistic values for material parameters. These results jointly with earlier ones[19] facilitated in determining that oxygen vacancies act as charge carrier traps.

Our results can be used to predict the leakage currents in HfO_2-based devices and applications. High-quality MOSFET and FinFET transistors and SONOS flash memory require low leakage currents through the gate dielectrics and blocking insulator, while different states in resistive memory cells must be distinguishable over a wide range of temperatures. Temperature dependence of memory window (resistance ratio in different states) in resistive memory might be predicted as well.

[1]T. P. Ma, H. M. Bu, X. W. Wang, L. Y. Song, W. He, M. Wang, H.-H. Tseng, and P. J. Tobin, IEEE Trans. Device Mater. Reliab. **5**, 36 (2005).

[2]J. Robertson, Rep. Prog. Phys. **69**, 327 (2006).

[3]M. A. Pavanello, J. A. Martino, E. Simoen, R. Rooyackers, N. Collaert, and C. Claeys, Solid-State Electron. **51**, 285 (2007).

[4]A. Tsormpatzoglou, D. H. Tassis, C. A. Dimitriadis, M. Mouis, G. Ghibaudo, and N. Collaet, Semicond. Sci. Technol. **24**, 125001 (2009).

[5]L.-J. Chen, Y.-C. Wu, J.-H. Chiang, M.-F. Hung, C.-W. Chang, and P.-W. Su, IEEE Trans. Nanotechnol. **10**, 260 (2011).

[6]P.-H. Tsai, K.-S. Chang-Liao, T.-C. Liu, T.-K. Wang, P.-J. Tzeng, C.-H. Lin, L. S. Lee, and M.-J. Tsai, IEEE Electron Device Lett. **30**, 775 (2009).

[7]J. J. Yang, M. D. Pickett, X. Li, D. A. A. Ohlberg, D. R. Stewart, and R. S. Williams, Nat. Nanotechnol. **3**, 429 (2008).

[8]L. Goux, P. Czarnecki, Y. Y. Chen, L. Pantisano, X. P. Wang, R. Degraeve, B. Govoreanu, M. Jurczak, D. J. Wouters, and L. Altimime, Appl. Phys. Lett. **97**, 243509 (2010).

[9]Z. Wang, H. Y. Yu, X. A. Tran, Z. Fang, J. Wang, and H. Su, Phys. Rev. B **85**, 195322 (2012).

[10]S. Yu, X. Guan, and H.-S. P. Wong, Appl. Phys. Lett. **99**, 063507 (2011).

[11]S. Guha and V. Narayanan, Phys. Rev. Lett. **98**, 196101 (2007).

[12]D. Muñoz Ramo, A. L. Shluger, J. L. Gavartin, and G. Bersuker, Phys. Rev. Lett. **99**, 155504 (2007).

[13]A. S. Foster, F. Lopez Gejo, A. L. Shluger, and R. M. Nieminen, Phys. Rev. B **65**, 174117 (2002).

[14]J. X. Zheng, G. Ceder, T. Maxisch, W. K. Chim, and W. K. Choi, Phys. Rev. B **75**, 104112 (2007).

[15]D. Muñoz Ramo, J. L. Gavartin, A. L. Shluger, and G. Bersuker, Phys. Rev. B **75**, 205336 (2007).

[16]H. Jiang, R. I. Gomez-Abal, P. Rinke, and M. Scheffler, Phys. Rev. B **81**, 085119 (2010).

[17]K. Xiong, J. Robertson, M. C. Gibson, and S. J. Clark, Appl. Phys. Lett. **87**, 183505 (2005).

[18]P. Broqvist and A. Pasquarello, Appl. Phys. Lett. **89**, 262904 (2006).

[19]T. V. Perevalov, V. S. Aliev, V. A. Gritsenko, A. A. Saraev, V. V. Kaichev, E. V. Ivanova, and M. V. Zamoryanskaya, Appl. Phys. Lett. **104**, 071904 (2014).

[20]S. K. Sahoo and D. Misra, J. Appl. Phys. **110**, 084104 (2011).

[21]S. Pan, S.-J. Ding, Y. Huang, Y.-J. Huang, D. W. Zhang, L.-K. Wang, and R. Liu, J. Appl. Phys. **102**, 073706 (2007).

[22]W. J. Zhu, T.-P. Ma, T. Tamagawa, J. Kim, and Y. Di, IEEE Electron Device Lett. **23**, 97 (2002).

[23]S. D. Ganichev, E. Ziemann, W. Prettl, I. N. Yassievich, A. A. Istratov, and E. R. Weber, Phys. Rev. B **61**, 10361 (2000).

[24]D. S. Jeong and C. S. Hwang, Phys. Rev. B **71**, 165327 (2005).

[25]S. H. Lin, C. H. Cheng, W. B. Chen, F. S. Yeh, and A. Chin, IEEE Electron Device Lett. **30**, 999 (2009).

[26]J. Frenkel, Phys. Rev. **54**, 647 (1938).

[27]R. M. Hill, Philos. Mag. **23**, 59 (1971).

[28]S. Makram-Ebeid and M. Lannoo, Phys. Rev. B **25**, 6406 (1982).

[29]K. A. Nasyrov and V. A. Gritsenko, J. Appl. Phys. **109**, 093705 (2011).

[30]H. Takeuchi, D. Ha, and T.-J. King, J. Vac. Sci. Technol., A **22**, 1337 (2004).

[31]K. A. Nasyrov, V. A. Gritsenko, Y. N. Novikov, E.-H. Lee, S. Y. Yoon, and C. W. Kim, J. Appl. Phys. **96**, 4293 (2004).

[32]L. Vandelli, A. Padovani, L. Larcher, R. G. Southwick, W. B. Knowlton, and G. Bersuker, IEEE Trans. Electron Devices **58**, 2878 (2011).

[33]D. R. Islamov, V. A. Gritsenko, C. H. Cheng, and A. Chin, Appl. Phys. Lett. **99**, 072109 (2011).

[34]T. Ando, N. D. Sathaye, K. V. R. M. Murali, and E. A. Cartier, IEEE Electron Device Lett. **32**, 865 (2011).

[35]V. V. Afanas'ev and A. Stesmans, J. Appl. Phys. **102**, 081301 (2007).